Effects of thickness on the cation segregation in epitaxial (001) and (110) $La_{2/3}Ca_{1/3}MnO_3$ thin films

S. Estradé,[1,a)] J. M. Rebled,[1] J. Arbiol,[1] F. Peiró,[1] I. C. Infante,[2] G. Herranz,[2] F. Sánchez,[2] J. Fontcuberta,[2] R. Córdoba,[3] B. G. Mendis,[4] and A. L. Bleloch[4]
[1]*Departament d'Electrònica, MIND-IN2UB, Universitat de Barcelona, c/Martí i Franquès 1, 08028 Barcelona, Catalonia, Spain*
[2]*Institut de Ciència de Materials de Barcelona, CSIC, 08193 Bellaterra, Catalonia, Spain*
[3]*Instituto Universitario de Investigación en Nanociencia de Aragón (INA), c/Pedro Cerbuna 12, 50009 Zaragoza, Spain*
[4]*SuperSTEM Laboratory, STFC Daresbury, Daresbury WA4 4AD, United Kingdom*

(Received 14 July 2009; accepted 1 August 2009; published online 21 August 2009)

Electron-energy-loss spectroscopy is used to map composition and electronic states in epitaxial $La_{2/3}Ca_{1/3}MnO_3$ (LCMO) films of various thicknesses grown on $SrTiO_3$ (001) and (110) substrates. For relatively thick films ($\geq$20 nm), epitaxial tensile strain in (001) films promotes a compositional La/Ca gradient across the film thickness, being the interface La rich, while the relaxed (110) films are chemically homogeneous. In contrast, much thinner (001) and (110) LCMO films display a different La/Ca distribution, being La rich at the free surface. The observed distinct thickness-dependent composition gradient behavior reflects a balance between strain-induced elastic energy minimization and kinetic effects during growth. © *2009 American Institute of Physics*. [DOI: 10.1063/1.3211130]

Mixed-valence ferromagnetic manganite films have been the object of much attention in recent years due to their potential applications in spintronics.[1,2] However, expectations have been lowered by the negligible room-temperature magnetoresistance observed in tunnel junctions.[3] Although the reasons for this behavior are not yet fully known, it has been suggested that they may be linked to electronic phase separation.[4] Whether the latter is a pure electronic effect or related to inhomogeneous chemical distributions can be suitably explored by electron energy-loss spectroscopy (EELS). For instance, electronic states can be mapped out by direct determination of local Mn oxidation state at the nanometric scale.[5–8] On the other hand, mappings of the chemical composition can be achieved offering chemical information at the nanometric scale[5–9]

We recently reported[8] a comparative characterization, both from the microstructural and chemical points of view, of relatively thick (~80 nm) LCMO layers grown on STO in order to determine which differences accounted for the fact that (110) LCMO films display enhanced magnetic properties when compared to their (001) counterparts. While homogeneous chemical composition was associated to the contribution of plastic defects as strain-relieve mechanism in the more relaxed (110) films, a Ca^{2+} ion migration toward free surface, and the concomitant Mn^{m+} oxidation state variation was observed in the more stressed (001) films.

In this letter, we have extended the characterization of the microstructure, local stoichiometry variations, and Mn oxidation state of (001) and (110) LCMO films within a range of layer thicknesses between 3.5 and 40 nm. The results confirm the same trend for LCMO films with $t \sim 40$ nm as those with $t \sim 80$ nm previously reported.[8] However, most importantly, we assess that for ultrathin LCMO films ($t < 20$ nm), a new scenario is revealed with significant differences regarding cation distribution across the film in comparison with thicker layers, while keeping an orthorhombic crystalline phase in contrast with structural changes reported by Qin *et al.*[10]

The (001) and (110) LCMO films with thicknesses (t) ranging from 3.5 to 82 nm were grown by rf sputtering at 800 °C, at 330 mtorr, with an O_2/Ar pressure ratio of 1/4 and a growth rate of ~0.4 nm/min for thicker samples (~80 and ~40 nm) and ~0.3 nm/min for the thinner ones. After growth, samples were *in situ* annealed at 800 °C for 1 h in O_2 atmosphere at 350 torr. Although already reported,[8] some results concerning the layers of $t=80$ nm are also included for the sake of completeness.

Transmission electron microscopy (TEM) samples, were prepared for cross section view by Dual Beam system from FEI (focused ion beam (FIB)/scanning electron microscope], and for plane-view (PV) geometry by mechanical thinning down to 25 μm and Ar^+ bombardment at $V=5$ kV and 7° using a PIPS-Gatan. They were observed in a Jeol J2010F scanning TEM (STEM) microscope, with a hot field emission gun at 200 keV, coupled with a GIF spectrometer with a 0.8 eV energy resolution. Additional EEL spectra and STEM images were obtained in a Nion UltraSTEM 100 aberration corrected dedicated STEM, with an energy resolution of 0.3 eV. Ca, La, and Mn normalized σ-weighted intensities were obtained from EELS spectra as I_x/σ_x, (where x is Ca, La, or Mn), normalized to the value of the mean Mn σ-weighted intensity along the layers. I_x are the integrated intensities of background subtracted Ca $L_{3,2}$, La $M_{5,4}$, and Mn $L_{3,2}$ edges, and σ_x is the cross section for each edge (calculated using Gatan DIGITALMICROGRAPH software). The Mn L_3 EELS edge position and Mn L_3/Mn L_2 edge intensity ratio were determined using MANGANITAS software package.[7,8]

Lattice parameter obtained from x-ray diffraction (XRD) reciprocal space maps[11] show that for both (001) and (110) films, the out-of-plane cell parameters in thinnest films (t

a)Electronic mail: sestrade@el.ub.es.

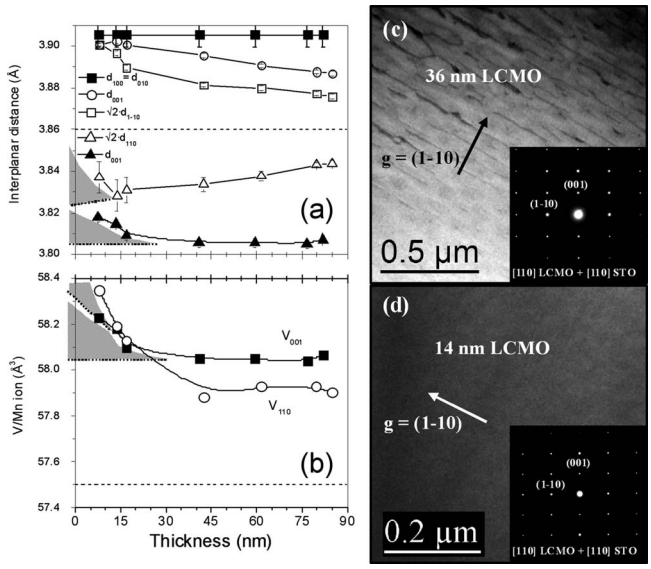

FIG. 1. (a) Out-of-plane and in-plane lattice parameters and (b) unit cell volume of (001) and (110) LCMO films as a function of the layer thickness. $\mathbf{g}=(1-10)$ bright field two-beam images of (c) 36 nm and (d) 14 nm thick (110) LCMO films in PV geometry. Insets: on-axis electron diffractions corresponding to the 36 and 14 nm, respectively, (110) films in PV geometry.

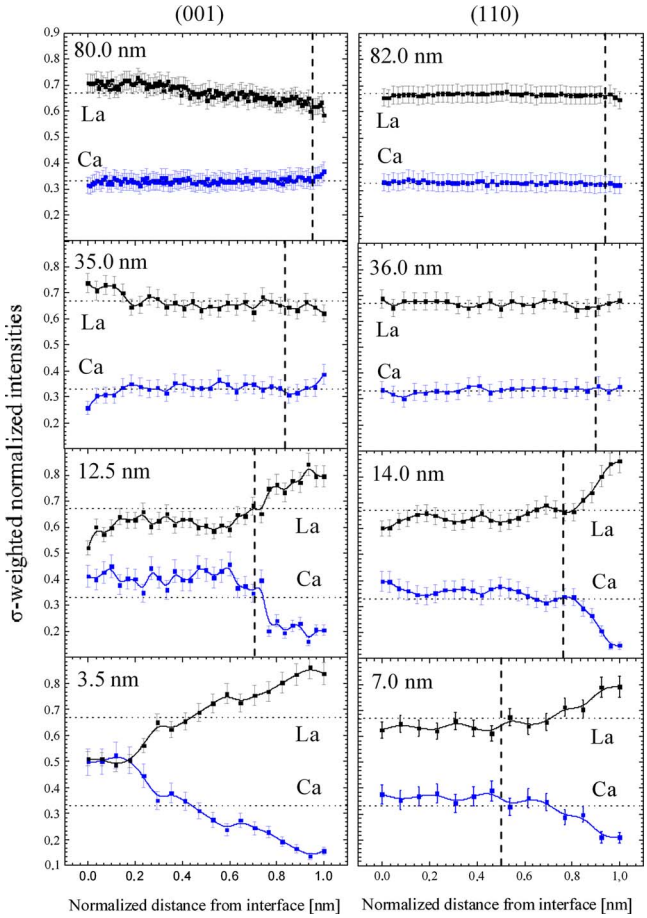

FIG. 2. (Color online) Ca and La and σ-weighted intensities as a function of normalized distance to interface for several film thicknesses for (a) (001) and (b) (110) LCMO films. Dashed lines indicate the outmost 3.5 nm of each film.

<20 nm) are substantially larger than expected [Fig. 1(a)] and the unit cell volume is also abnormally large [Fig. 1(b)]. In Figs. 1(c) and 1(d) we show TEM PV bright field two-beam images of the $t\approx 36$ and 14 nm (110) LCMO films, respectively. Plastic relaxation was evident for (110) thicker ($t>20$ nm) films [Fig. 1(c)]. In contrast, PV images of the thinnest ($t<20$ nm) (001) and (110) films yields no evidence of misfit dislocations [Fig. 1(d)]. Thus, $t<20$ nm LCMO layers are dislocation free irrespective of their orientation. Moreover, TEM characterization of these thin films shows no crystal symmetry change with respect to thicker films. The insets in Figs. 1(c) and 1(d) display on-axis electron diffractions corresponding to the 36 and 14 nm, respectively, (110) films in PV geometry.

Composition profiles across film thickness were obtained by EELS from FIB lift-off cross section foils. In order to evaluate the suitability of the FIB lamellas for EELS experiments, foil thicknesses (t_s) were estimated from low loss spectra via log-ratio calculations. All t_s were found to fall within the $(20\pm 2)-(32\pm 3)$ nm range. General spectra (in the range of 325–870 eV) were acquired along the direction perpendicular to the substrate/film interface. Concentrations of the different elements at different positions were determined from these spectra. Ca and La and σ-weighted intensities along the layers are depicted for (001) and (110) films of various thicknesses, in Fig. 2. Depending on the thickness, two distinct regimes are evident. For $t>20$ nm, (110) and (001) layers present a clearly different behavior. While in (110) films the Ca, and La concentrations are found to be constant and close to the expected values—0.33 and 0.66—across the whole film, this is not the case of the (001) films where a monotonous reduction of the La intensity across film thickness is found, the interface being La enriched and the free surface, La deficient. Accordingly, the Ca intensity increases with distance to interface. In sharp contrast, for $t<20$ nm, irrespective of layer orientation, the free surface gets progressively La rich (Ca deficient) as thickness is reduced. The effect is somewhat more pronounced in the (001) films than in (110). It is worth noticing that the total [(Ca+La)/Mn] ratio remains constant, around the expected proportion of ~ 1, for all the considered samples. No overall cation deficiency is thus observed.

EELS spectra in the 400–750 eV energy-loss range, where Mn $L_{2,3}$ edges (640 and 651 eV, respectively) and O K edge (532 eV) occur, were also recorded. In Fig. 3(a), representative individual EEL spectra are given for illustration purposes. The position of the Mn L_3 edge is well known to be related to the Mn oxidation state.[12–14] In Fig. 3(b) we report the Mn L_3 edge position along the layer (from interface to free surface) for (001) and (110) layers of different thicknesses. Dotted lines in Fig. 3(b) indicate the Mn L_3 edge positions reported in literature for Mn^{2+}, Mn^{3+}, and Mn^{4+} ions.[12] Two thickness regimes are observed once more. For thicker (110) films, no significant variation is found to take place along the layer. Yet, the oxidation state of Mn^{m+} ions gradually changes in (001) thick films, with a progressive reduction in the Mn^{m+} species near the interface while free surface is overoxidized. This observation is consistent with the La^{3+} enrichment of the free surface described before (Fig. 2) and it is in agreement with early results.[8] In contrast, in Fig. 3(a) it can be appreciated that for the thinnest samples the Mn^{m+} ions get progressively more reduced when approaching the free surface. Local Mn oxidation state as determined by L_3/L_2 edge intensity ratio (not displayed here) is

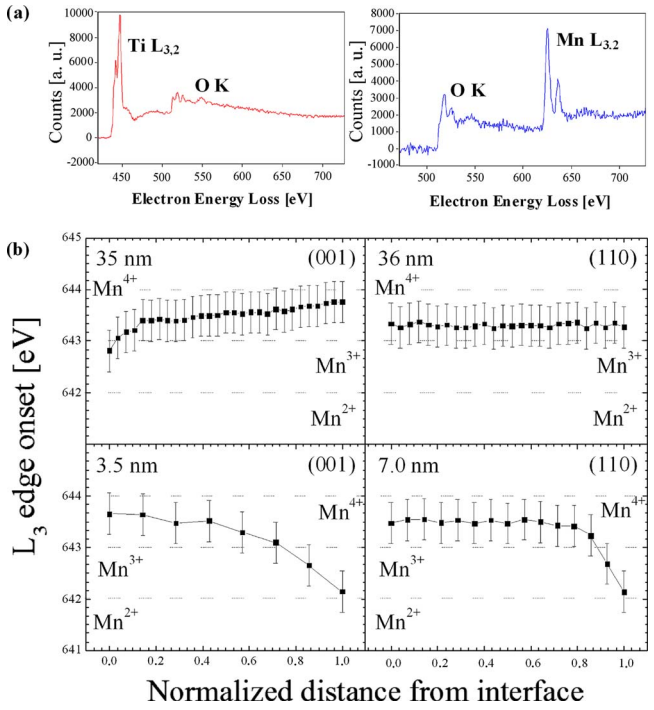

FIG. 3. (Color online) (a) Representative individual EEL spectra obtained at the STO substrate (left panel) and at the LCMO layer. (b) Mn L_3 peak onset as a function of normalized distance to interface in representative (001) and (110) LCMO films.

coherent with the one obtained through L_3 onset position data for all samples. The observed variation in Mn^{m+} oxidation state in the thinnest (001) and (110) films is fully consistent with the detected La enrichment near the free surface. Yet, for thinner films, Mn seems to be more reduced than it should be expected from the Ca/La proportion data.

In Fig. 4, the O σ-weighted intensity along the layers is depicted, for (001) and (110) films of various thicknesses. For thicker layers, the O intensity remains constant across the film; the [O/Mn] concentration ratio is found to be close to the expected value (~3). In contrast, for the thinner films, the oxygen concentration is not constant but a significant decrease is observed close to the substrate/film interface

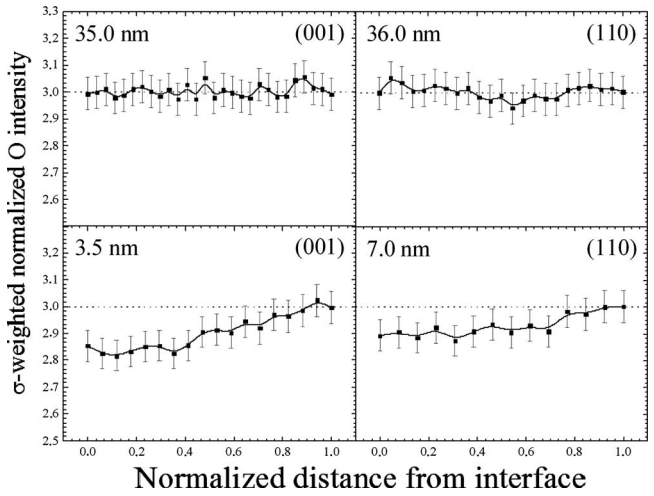

FIG. 4. O σ-weighted intensity as a function of normalized distance to interface in representative for (001) and (110) LCMO films.

In view of TEM, EELS, and XRD results two different regimes are revealed. Data of samples of $t \sim 40$ nm are in very good agreement with those of thicker layers ($t \sim 80$ nm) previously reported,[8] thus supporting the identified stress accommodation mechanisms for (001) and (110) LCMO films grown on STO,[8] namely, Ca cation migration toward free surface (and concomitant Mn oxidation state variation) for (001) LCMO films and plastic relaxation for (110) LCMO orientation. The self-adapting chemical variation related to strain-induced elastic energy is the prevalent mechanism for chemical-phase separation only for (001) films thicker than a critical value which is about ~20 nm for LCMO/STO. For thicknesses below this threshold, a different behavior emerges: La migration toward free surface occurs in absence of plastic relaxation irrespective of LCMO orientation. Both this cation distribution and the apparition of O vacancies, mostly near the interface, determine the Mn^{m+} oxidation state. The presence of O vacancies would account for the abnormally large unit cell volume detected by XRD for the thinnest layers. For this ultrathin regime for which elastic energy considerations should not be the determinant, kinetic factors such as cation incorporation rate, i.e., sticking coefficient and growth parameters, would determine the local chemistry of the layers.

Financial support from the Ministerio de Ciencia e Innovación of the Spanish Government Projects (Grant Nos. MAT2008-06761-C03 and NANOSELECT CSD2007-00041) and from the European Union [Project MaCoMuFi (Grant No. FP6-03321) and FEDER] is acknowledged. We acknowledge the TEM facilities of Science and Technical Services of Universitat de Barcelona (SCT-UB). We also acknowledge Nanoaracat Aragon-Catalonian cooperation program and ESTEEM.

[1] J. S. Moodera and G. Mathon, J. Magn. Magn. Mater. **200**, 248 (1999).
[2] S. S. P. Parkin, K. P. Roche, M. G. Samant, P. M. Rice, R. B. Byers, R. E. Scheuerlein, E. J. O'Sullivan S. L. Brown, J. Bucchigano, D. W. Abraham, Yu Lu, M. Rooks, P. L. Trouilloud, R. A. Wanner, and W. J. Gallagher, J. Appl. Phys. **85**, 5828 (1999).
[3] M. Viret, M. Drouet, J. Nassar, J. P. Contour, C. Fermon, and A. Fert, Europhys. Lett. **39**, 545 (1997).
[4] M. Bibes, Ll. Balcells, S. Valencia, J. Fontcuberta, M. Wojcik, E. Jedryka, and S. Nadolski, Phys. Rev. Lett. **87**, 067210 (2001).
[5] M. Varela, M. M. P. Oxley, W. Luo, J. Tao, M. Watanabe, A. R. Lupini, S.T. Pantelides, and S.J. Pennycook, Phys. Rev. B **79**, 085117 (2009).
[6] J.-L. Maurice, D. Imhoff, J.-P. Contour, and C. Colliex, Philos. Mag. **86**, 2127 (2006); L. Samet, D. Imhoff, J.-L. Maurice, J.-P. Contour, A. Gloter, T. Manoubi, A. Fert, and C. Colliex, Eur. Phys. J. B **34**, 179 (2003).
[7] S. Estradé, J. Arbiol, F. Peiró Ll. Abad, V. Laukhin, Ll. Balcells, and B. Martínez, Appl. Phys. Lett. **91**, 252503 (2007).
[8] S. Estradé, J. Arbiol, F. Peiró, I. C. Infante, F. Sánchez, J. Fontcuberta, F. de la Peña, M. Walls, and C. Colliex, Appl. Phys. Lett. **93**, 112505 (2008).
[9] J. Simon, T. Walther, W. Mader, J. Klein, D. Reisinger, L. Alff, and R. Gross, Appl. Phys. Lett. **84**, 3882 (2004).
[10] Y. L. Qin, H. W. Zandbergen, Z. Q. Yang, and J. Aarts, Philos. Mag. **85**, 4465 (2005).
[11] I. C. Infante, F. Sánchez, J. Fontcuberta, M. Wojcik, E. Jedryka, S. Estradé, F. Peiró, J. Arbiol, V. Laukhin, and J. P. Espinós, Phys. Rev. B **76**, 224415 (2007).
[12] H. Kurata and C. Colliex, Phys. Rev. B **48**, 2102 (1993).
[13] L. Garvie and A. Craven, Ultramicroscopy **54**, 83 (1994).
[14] H. K. Schmid and W. Mader, Micron **37**, 426 (2006).